The place of the local group in the cosmic web

Sebastian Bustamante $^{\star 1}$ Jaime E. Forero-Romero^2

^{1}*Instituto de Física - FCEN, Universidad de Antioquia, Calle 67 No. 53-108, Medellín, Colombia*
^{2}*Departamento de Física, Universidad de los Andes, Cra. 1 No. 18A-10, Edificio Ip, Bogotá, Colombia*

30 October 2013

ABSTRACT

We present here a study about the influence of the environment on the local group (LG) of galaxies in the context of ΛCDM. In this study we use a large volume high resolution N-body cosmological simulation (Bolshoi) together with the most recent methods to quantify the cosmic web (T-web, V-web schemes); furthermore we propose a novel approximation, base upon the minimization of the mean density of void regions, to determinate the optimal threshold value λ_{th}, which have been treated until now as a free parameter. Following the recent work of Courtois et al. (2013), where was found that the LG is located near to a large void, we also do an extensive study of voids, applying a FOF algorithm to find void regions and performing an analysis of their shape based upon the reduced inertia tensor. Using the recent observations that constrained the tangential velocity of M31 with respect to the Milky Way (MW), the previously established radial velocity, the estimated masses of dark halos, along with some criteria to guarantee the gravitational isolation of these systems (Forero-Romero et al. 2013-1), we select a set of halos pairs as a representative sample of LG-like systems in the Bolshoi simulation. We look for possible bias and correlations between the environment properties of each LG-like system and its kinematic and formation properties. Among our main result we find [**summarize our results here!**].

Key words: Cosmology: large-scale Structure of Universe, galaxies: star formation - line: formation

1 INTRODUCTION

The spatial distribution of galaxies describes a web-like pattern, the so-called cosmic web. Today it is understood that such configuration is driven by gravitational instabilities. ...

The study of the influence of the cosmic web on galaxy properties start with the seminal work of Dressler [**reference here**] and extends to recent works using large observational surveys that look for signatures of the web into the evolution of galaxy populations. With the advent of more detailed observations and sophisticated computational models it is now within our reach to understand what physical processes dominate.

This makes that the mass assembly history of a galaxy is deeply connected with its position in the cosmic web. There is an extensive body of literature on the effects of the web environment on the observable properties of galaxies.

This environmental study is also of paramount importance to understand the formation of our Galaxy. In our local neighborhood, the observations of dwarf galaxies around the Milky Way (MW) and the Andromeda galaxy (M31) show filamentary and disk-like patterns that can be linked to a preferential infall direction, very likely connected with the cosmic web where the Local Group (LG) of galaxies is embedded.

In this paper we quantify the velocity shear environment of DM halo pairs representative of the principal members of the Local Group (LG), the Milky Way (MW) and Andromeda galaxy (M31). We perform this study in an unconstrained cosmological simulation from random phases in the initial conditions, and unlike previous works, where were used constrained cosmological simulations which have been setup as to reproduce the large scale structure of the local universe, we use directly observational measurements of the kinematics properties of the local group [**Reference here**] in order to build faithful samples of LG-like systems.

We pay special attention to the correlation of the present velocity shear environment with the assembly and the kinematics properties of the pairs. The motivation to have that focus is that it has been previously shown that the LG present in three different realizations of the constrained simulations have assembly histories biased towards

---

* sbustama@pegasus.udea.edu.co

early formation times and absence of major mergers (ratio 1:10) in the last 10 Gyr. In the case of the kinematic properties, recent observational constrains to the galactocentric tangential velocity of M31 has enabled to establish how typical is the LG in a cosmological context [**reference to Forero-Romero et.al 2013-1**], that is why we focus here how a specific kind of host environment biases these kinematics properties.

2   THE SIMULATION

As it was previously mentioned, we use an unconstrained cosmological simulation, the Bolshoi simulation, to identify the possible large scale environment of the Local Group. This is a similar approach to the one already used by [**reference here**].

The Bolshoi simulation follows the non-linear evolution of a dark matter density field on a cubic volume of size $250h^{-1}$Mpc sampled with 2048^3 particles. The cosmological parameters in the simulation are $\Omega_{\rm m} = 0.27$, $\Omega_\Lambda = 0.73$, $h = 0.70$, $n = 0.95$ and $\sigma_8 = 0.82$ for the matter density, cosmological constant, dimensionless Hubble parameter, spectral index of primordial density perturbations and normalization for the power spectrum. The mass of each particle in the simulation is $m_{\rm p} = 1.4 \times 10^8 h^{-1}{\rm M}_\odot$.

2.1   Halos and Merger Trees

We identify halos with two algorithms, the Friends-of-Friends [**reference here**] algorithm and the Bound Density Maximum algorithm. The constructed catalogues also provide the basis for the mass aggregation history studies. We also include in the catalogues information about the substructure.

All the results presented here must be interpreted in term of host halos, without any information of the substructure. In particular the merger of two FOF halos corresponds to the epoch of first overlap, and not to the fusion and/or disruption of an accreted sub-halo with a dominant halo.

The linking length is $b = 0.17$ times the mean interparticle separation. All objects with 20 particles or more are considered a bona fide halo and are included in the construction of the merger tree, this corresponds to a minimum halo mass of $M_{\rm min} = 2.70 \times 10^9 h^{-1}{\rm M}_\odot$ in the Bolshoi simulation.

The halo identification for the simulation was done for XX snapshots in the redshift range $0 < z < 7$ more or less evenly spaced in look-back time.

3   ALGORITHMS TO QUANTIFY THE COSMIC WEB

3.1   The tidal web (T-web)

The first algorithm we use to identify the cosmic web is based upon the diagonalization of the tidal tensor, defined as the Hessian of a normalized gravitational potential

$$T_{\alpha\beta} = \frac{\partial^2 \phi}{\partial x_\alpha \partial x_\beta} \qquad (1)$$

where the physical gravitational potential has been rescaled by a factor $4\pi G\bar\rho$ in such a way that ϕ satisfies the following equation

$$\nabla^2 \phi = \delta, \qquad (2)$$

where $\bar\rho$ is the average density in the Universe, G is the gravitational constant and δ is the dimensionless matter overdensity.

3.2   The velocity web (V-web)

We also use a kinematical method to define the cosmic-web environment in the simulation. The method has been thoroughly described in XXX and applied to study the shape and spin alignment in the Bolshoi simulation here XX. We refer the reader to these papers to find a detailed description of the algorithm, its limitations and capabilities. Here we summarize the most relevant points for the discussion.

The V-web method for environment finding is based on the local shear tensor calculated from the smoothed DM velocity field in the simulation. The central quantity is the following dimensionless quantity

$$\Sigma_{\alpha\beta} = -\frac{1}{2H_0}\left(\frac{\partial v_\alpha}{\partial x_\beta} + \frac{\partial v_\beta}{\partial x_\alpha}\right) \qquad (3)$$

where v_α and x_α represent the α component of the comoving velocity and position, respectively. $\Sigma_{\alpha\beta}$ can be represented by a 3×3 symmetric matrix with real values, that ensures that is possible to diagonalize and obtain three real eigenvalues $\lambda_1 > \lambda_2 > \lambda_3$ whose sum (the trace of $\Sigma_{\alpha\beta}$) is proportional to the divergence of the local velocity field smoothed on the physical scale $\mathcal{R}$.

The relative strength of the three eigenvalues with respect to a threshold value λ_{th} allows for the local classification of the matter distribution into four web types: voids, sheets, filaments and peaks, which correspond to regions with 3, 2, 1 or 0 eigenvalues with values larger than λ_{th}. Below we shall discuss a novel approach to define an adequate threshold value based on the visual impression of void regions, furthermore we study other possible values based on other visual features of the cosmic web.

3.3   The cosmic web in Bolshoi

Both established schemes to quantify the cosmic web depend on continuous and smooth physical quantities, as the peculiar velocity field and the density field. In order to calculate the necessary tensors, a discretization of the simulation volume is performed, so all the properties are reduced to single values associated to discrete cells. According to this, we divide the overall volume into $(256)^3$ cells, so each cell has an associated comoving cubic volume of 0.98 Mpc h^{-1}. Finally, in order to reduce possible effects due to the discretization process, a gaussian softening is performed between neighbour cells.

Once defined the numerical details about the classification schemes, we shall analyse the dependence on the threshold value λ_{th} for each one. In Figure 1 we show the variation of the mean density parameter δ with the threshold value

for cells marked as one of the two more dominant types of environment (voids and sheets).

As was previously established by **Hoffman et al. (2012)** and as can be seen in Figure 1, the behaviour of the V-web scheme is significantly more sensible to variations of the λ_{th} value compared with the T-web scheme; nevertheless, the behaviour of the mean density parameter for voids, sheets and filaments, are qualitatively quite similar for the two schemes, increasing with the value of λ_{th}. Although we shall focus our analysis on voids because they are completely dominant in the visual impression of the cosmic web, an analogous analysis might be performed for other type of environments.

On cosmic scales, the presence of highly non-linear structures implies the existence of very vast regions with density lower than the mean cosmological value due to the mass conservation. That is why the visual impression of the cosmic web must be necessarily dominated by these underdense regions. Keeping that in mind, our novel proposal is based upon the correct quantification of these regions, so the optimal threshold value must be chosen such that: sheet regions do not invade real void regions (in such case, the mean density parameter of sheet regions would become negative) and void regions do not invade real sheet and filament regions (in such case, the mean density parameter of void regions would increase due to the contribution of over-dense regions). Thus, the optimal value is simply where the mean density parameter of sheet regions is null. According to this, we obtain the next optimal threshold values for the T-web and the V-web respectively, $\lambda_{opt}^T = 0.326$ and $\lambda_{opt}^V = 0.188$. To verify our analysis, we show in Figure 2 the visual impression for each defined critical value, and as can be seen, the chosen values reproduce properly the expected impression according to the density field.

Our classification scheme may be thought as a refinement of the recent schemes, where the threshold value is used to taking as a free parameter, based on the classic methods, where the classification is performed based on a cut off of the density field directly [**references here**]. So we make use of the objectivity achieved by the analysis of the mean density, but keeping all the environmental information provided by the tensorial schemes instead of the poor description provided by the density field.

3.4 Method to find void regions

Following the recent work of **Courtois et al. 2013**, we use a method based on a FOF-like algorithm to find extended regions of voids in order to select halo systems according to the proximity to those regions. To achieve this, we build the input catalogue of the FOF method with the positions of the center coordinate of every cell marked as void according to the web scheme adopted; furthermore we set an adequate linking length to connect even diagonal neighbour cells.

Following the work of **Forero-Romero et al. 2008**, we also perform a percolation analysis in order to select the best threshold parameter that reduce percolation in cells, thereby accounting for physical void regions. In Figure 3 we show the obtained result of our percolation analysis for both web schemes. In both cases it can be noted the volume of the largest void region is minimized and the volume distribution of voids is relatively flat at $\lambda_{th} = 0.0$, that means percolation

is completely reduced for this threshold value. So despite of the previously established λ_{th} optimal values for each scheme, we shall use $\lambda_{th} = 0.0$ just for the detection of void regions. Besides, due to the domination of the large scale visual impression by voids, it is inevitable the presence of percolation phenomenon, so the current chosen threshold value for percolation is justified because in spite of voids are necessarily connected, we are just interested in detecting bulk regions.

Next, we shall calculate the reduced inertia tensor of each void region in order to determinate their principal directions of inertia and analyse the size-shape distribution of voids.

$$\tau_{ij} = \sum_l \frac{x_{l,i} x_{l,j}}{R_l^2} \tag{4}$$

where l is a index associated to each cell of to the current region, i and j indexes run over each spatial direction and finally R_l is defined as $R_l^2 = x_{l,1}^2 + x_{l,2}^2 + x_{l,3}^2$, all positions are measured from the respective center of mass of the region.

The eigenvalues of the reduced inertia tensor, i.e. the principal moments of inertia, are used to quantify the shape of void regions. They are denoted as τ_1, τ_2 and τ_3 such that $\tau_1 \leq \tau_2 \leq \tau_3$. In Figure 4 we show the computed distributions for τ_1/τ_2 and τ_2/τ_3, where we rather calculate histograms for these ratio quantities instead of each value in order to avoid using an arbitrary normalization. For both schemes, it can be noticed that the shape-distribution is completely spread out, thereby indicating a non-preferred geometry of void regions, which is in agreement with the well-established anisotropic flow of matter associated to this type of region [**reference here**]. Because of that, we shall look for possible alignments between the plane of rotation of halo pairs and the principal directions of inertia of the nearest void regions.

4 DEFINING SAMPLES

In order to establish an adequate set of criteria to define a LG-like sample in unconstrained simulations, we proceed from the the general dark halo catalogues, constructed using the FOF scheme with a linking length of $b = 0.17$ and the Bound Density Maxima (BDM) scheme for halos with an associated overdensity value of 200 times the critical density ([**references here**]). These samples are defined over all the Bolshoi simulation and will be referred as General Halos samples, $\texttt{GH}_{\text{FOF}}$ and $\texttt{GH}_{\text{BDM}}$ respectively[1]. To be consistent with the mass range observationally determined of halos that host disk-form galaxies, we select halos in the mass range $7 \times 10^{11} < M_h/h^{-1} \text{M}_\odot < 7 \times 10^{12}$, referred here as Individual Halos (IH) samples.

As a primal approach to define gravitational bounded halo pairs we select halos within the IH sample that satisfied to be the closest to each other. They constitute the Pairs (P) sample. To maintain the consistency with previous works regarding algorithms used for LG selection ([**references here**]), we define here the next list of conditions that

---

[1] For each sample defined, there will be a FOF sample and a BDM sample in order to have robust results

have to fulfil a pair system in order to belong to the Isolated Pairs (IP) sample. All these considerations are based upon the relative dynamics of the Milky Way and M31, and its isolation from massive structures:

(i) With respect to each halo, there cannot be any other halo within the mass range $7 \times 10^{11} < M_h/h^{-1}\mathrm{M}_\odot < 7 \times 10^{12}$ closer than its partner. It means that there cannot be ambiguity on the identity of the pair members.

(ii) The relative radial velocity between the two halos must be negative.

(iii) The distance between the center of the two halos must be less than $1.0h^{-1}\mathrm{Mpc}$.

(iv) The distance to any halo more massive than any of the pair members cannot be less than $3h^{-1}\mathrm{Mpc}$.

(v) The distance to cluster-like halos with masses larger than $7 \times 10^{13}\ h^{-1}\mathrm{M}_\odot$ must be larger than $4h^{-1}\mathrm{Mpc}$.

Following the previous criteria established by Forero-Romero et al. 2013-1, we define a more reduced sample, the Reduced Isolated Pairs sample (RIP), as pairs that fulfil the next two extra criteria :

(i) The separation between the center of mass of the halos is in the range $700 - 800\mathrm{kpc}$.

(ii) The total mass of the two halos is in the range $1 - 4 \times 10^{12}/h^{-1}\mathrm{M}_\odot$.

Finally in Table 1 shows the sizes of all defined samples.

Sample	FOF	BDM
General Halos (GH)	432000	404432
Individual Halos (IH)	65109	61165
Pairs (P)	17115	15981
Isolated Pairs (IP)	1249	1647
Reduced Isolated Pairs (RIP)	138	116

Table 1: Size of each sample defined in the Bolshoi simulation and for each of the two schemes used to detect halos (FOF and BDM).

It can also be noticed both schemes used to detect halos in the simulation (henceforth halo schemes) are practically equivalent regarding the size of each sample.

5 FINDING THE ENVIRONMENT OF THE LOCAL GROUP

Once defined all samples, we shall proceed to quantify the environment by using two different approaches. The first one is by applying the tensorial schemes defined in Section 3 and then, calculating the local eigenvalues associated to each halo or halo pair and the respective fractional anisotropy index ([**reference here**]). The second approach is complementary to the first one, and consists in calculating the relative distance of each halo or halo pair to the nearest void regions, thereby allowing linking the influence of bulk voids to physical properties of the samples.

5.1 Tensorial Schemes

The advantage of using the tensorial schemes (T-web and V-web) defined in Section 3, lies in being able to quantify all the local structure of the environment of halos and pair halos just from kinematic and dynamic properties of the matter distribution, like the density and velocity fields. Next, we shall calculate the distributions of each eigenvalue for the two defined web schemes and for the GH, IP and RIP samples. In Figure 5 is shown the obtained results, where it can be noticed that there is a significant bias in the distribution of halo pairs respect to volume cells. Furthermore, choosing the previously established optimal threshold value λ_{opt} for each web scheme, Table 2 is built. In this has been listed the occupation fractions for the volume cells of the simulation and for each sample defined in the previous Section 4.

T-web				
Region	void	sheet	filament	knot
Cells	0.606	0.291	0.097	0.007
GH$_{\mathrm{FOF}}$	0.121	0.359	0.433	0.087
GH$_{\mathrm{BDM}}$	0.097	0.319	0.442	0.142
IP$_{\mathrm{FOF}}$	0.001	0.061	0.633	0.305
IP$_{\mathrm{BDM}}$	0.001	0.030	0.533	0.436
RIP$_{\mathrm{FOF}}$	0.000	0.051	0.884	0.065
RIP$_{\mathrm{BDM}}$	0.000	0.034	0.853	0.112

V-web				
Region	void	sheet	filament	knot
Cells	0.493	0.383	0.113	0.011
GH$_{\mathrm{FOF}}$	0.227	0.443	0.293	0.037
GH$_{\mathrm{BDM}}$	0.207	0.436	0.316	0.042
IP$_{\mathrm{FOF}}$	0.133	0.636	0.231	0.001
IP$_{\mathrm{BDM}}$	0.107	0.601	0.284	0.008
RIP$_{\mathrm{FOF}}$	0.203	0.681	0.116	0.000
RIP$_{\mathrm{BDM}}$	0.138	0.690	0.172	0.000

Table 2: Occupation fractions for each one of the defined samples and for all the volume cells of the simulation, and for each one of the occupied type of environment selected by both web schemes.

As it was said, the selection of a optimal threshold value for each web scheme, according to our proposed method based upon the mean density, is just an approximation which reproduces properly the visual impression of the cosmic web, so Table 2 must not be interpreted rigorously. Those occupation values must be thought just as a comparative illustration in order to understand possible bias between the defined samples and the overall matter distribution of the simulation. For instance, for T-web scheme, the occupation fraction of the RIP sample in filament regions is larger than

in sheet regions, which does not mean that `RIP` systems lie in filaments, but those systems lie preferentially in higher density and stronger non-linear regions.

An expected result obtained from Figure 5 is the equivalence between both used halo schemes, regarding the obtained distribution of eigenvalues for all samples, and even for both web schemes. This along with that shown in Table 1 allow concluding both halo schemes reproduce equivalent halos mass function and similar spatial distribution of them since the occupation values of each sample are approximately close. Regarding the differences between both web schemes, from the distribution of the web eigenvalues for volume cells shown by Figure 5 it is clear that each scheme quantify the structure of the cosmic web in very different ways, what can be explained by how each scheme is built. The T-web is built based upon the gravitational potential, thereby retaining bulk features of the cosmic web because of the long-range nature of the potential, whereas the V-web scheme, based upon the peculiar velocity field, describes better the very local structure of the cosmic environment. All of this causes filament-like and knot-like regions being poorly described by the T-web and hence being more spread out than the V-web. Voids and sheet-like regions are therefore more spread out in the V-web scheme. It must be noticed these conclusions were done independently on the chosen threshold value, and they hold for a reasonable range of them (see Figure 2).

Once established the expected characteristics of each web scheme, we shall proceed to analyse the privileged environment of LG-like systems under the selection criteria defined in Section 4. An interesting issue to be taken into account before, is the push and pull situation produced by the closeness criteria between the halos of each pair, and the gravitational isolation criteria. Correlation between the cosmic environment and the abundance and masses of individual galaxies has been well studied ([**references here**]), finding more massive galaxies and large abundances in high non-linear and denser regions of the cosmic web. This is in agreement with the closeness criteria, allowing finding more halos, but it is against the isolation criteria, where large abundances affect gravitational isolation. Because of that, it makes no clear how to assign a priori type of environment to LG-like systems, making this study necessary.

When we adopt the T-web scheme, an important bias is found for the `RIP` sample compared with the `IP`, whereas this one also follows a different distribution than the `GH` sample. According to Table 2, `RIP` systems appears to lie in high non-linear regions preferentially, with $\sim 85\% - 90\%$ being in filament-like regions, and $\sim 15\% - 10\%$ distributed in sheet-like and knot-like regions[2]. `IP` systems lie in even higher non-linear regions than `RIP` systems, with $\sim 30\% - 45\%$ of them distributed in knot-like, $\sim 63\% - 53\%$ in filament-like and the remainder distributed mainly in sheet-like regions.

Using the V-web scheme, there is also a bias between the environmental distribution of `RIP` and `IP` systems, but it is less clear than the T-web case. Furthermore, the occupation fractions are quite different to the T-web scheme.

For instance, `RIP` systems lie mainly in sheet-like regions, with $\sim 68\% - 69\%$ of them found in this type of region, $\sim 20\% - 14\%$ in voids and $\sim 12\% - 17\%$ in filament-like regions. Whereas there are $\sim 60\% - 63\%$ of *IP* systems in sheet-like regions, $\sim 28\% - 23\%$ in filament-like, $\sim 10\% - 13\%$ in voids and remainder in knot-like regions. All of this shows effectively a minor bias respect to that found in the T-web, what might be explained because of the different physical origin of each scheme.

5.2 Fractional anisotropy

In order to overcome and standardize differences between the two web schemes, we shall calculate the fractional anisotropy for each sample, with the normalization given by ([**reference here**]).

$$FA = \frac{1}{\sqrt{3}} \sqrt{\frac{(\lambda_1 - \lambda_3)^2 + (\lambda_2 - \lambda_3)^2 + (\lambda_1 - \lambda_2)^2}{\lambda_1^2 + \lambda_2^2 + \lambda_3^2}} \quad (5)$$

where the eigenvalues can be taken from any of the two web schemes. This index, such as it is defined, allows quantifying the local anisotropy degree of the cosmological environment, where $FA = 0$ corresponds to highly isotropic regions and $FA = 1$ the opposite case, completely anisotropic regions. Although there does not exist a perfect correspondence between certain range of the fractional anisotropy and each one of the above defined type of environment, there is an insight about what characteristics should have a cell volume according to its FA value. Following the analysis performed by ([**reference here**]), we shall assign low values of the fractional anisotropic to the most symmetric and isotropic regions, knot-like, due to their collapse in all directions. Low-middle values are assigned to sheet-like regions whereas high-middle values to filament-like regions, which indicates the complex dynamics of these types of environment. Finally, high values ($FA \lesssim 1$) of the fractional anisotropy correspond to the most highly anisotropic type of environment, voids. That is because their expansion rate in each direction can take very different values, thereby shaping highly amorphous regions.

Figure 6 shows the normed cumulative histograms of the fractional anisotropy for each sample. The first characteristic that can be noticed is the high similitude between both web schemes, allowing inferring that the fractional anisotropy is effectively an efficient way to overcome differences between the web schemes, and thereby allowing obtaining more robust conclusions. Regarding possible differences between each sample, now it is clearer the existing bias between `RIP` and `IP` systems, even for both web schemes. In spite of all the halos of the simulation are distributed mainly in very anisotropic regions like voids and sheet-like regions, `RIP` and `IP` systems lie preferentially in more isotropic and non-linear regions than `GH`. Although `RIP` systems appear to lie in slightly less isotropic regions. This can be explained because of the mass cut-off or the relative distance range chosen as the extra criteria for selecting the `RIP` sample, thus indicating a first possible environmental correlation. These conclusions reinforce the results obtained in previous Subsection 5.1, showing the complementary character of the fractional anisotropy.

---

[2] Note we rather use sheet-like, filament-like, ... regions instead of sheet, filament, ... regions in order to not classify a priori each type of region according to the optimal threshold value.

Returning back to the discussion about the quantification of the environment leaded by the fractional anisotropy, due to its fuzzy character, it is not possible to assign a well-defined type of environment to each sample. While this may be thought as a disadvantage of the method, actually the real character of the cosmological matter distribution is also fuzzy, where any attempt to stablish well-defined type of regions depends necessarily on free parameters like the threshold value λ_{th}, which has little or no physical motivation. So independence of free parameters is indeed and advantage of the fractional anisotropy.

5.3   The neighbourhood of voids

In Subsection 3.4 we quantified bulk void regions using a FOF-like scheme. Our second approach to quantify the cosmological environment of LG-like systems involves taking distances to the nearest void regions in order to stablish possible environmental effects related with the closeness, the size and the geometry of these bulk voids.

Figure 7 shows cumulative distributions of the distance to the nearest cell that belongs to the nearest void region from each one of the systems of each defined sample, and the volume size of such region. The first characteristic that can be noticed of this Figure is the lack of any bias between the defined samples, indicating there are no preferential locations regarding the spatial distribution of void regions and related with the selection criteria of pair systems.

When non-cumulative distributions are performed, we obtain a peak of distance to the nearest region, for all the samples, in $\sim 3h^{-1}$ Mpc, thereby indicating that most of the halos are spatially distributed relatively close to void regions. Nevertheless, distances in this context are meaningless because of the arbitrary origin of the chosen threshold value λ_{th} in Subsection 3.4, just to minimize the percolation phenomenon. Although this approach is just useful to quantify relative differences between the distribution of pair samples with regard to general halos, in next sections it may be useful in the frame of the analysis of other physical properties.

6   INFLUENCE OF THE ENVIRONMENT ON LG-LIKE SYSTEMS

Once defined the general features of the preferred environment of each pair sample, the next step is to look for possible environmental effects on all the physical properties of these systems. First, we shall study effects on kinematic properties like the total mass of the pair, radial and tangential velocities, angular momentum and total energy, and the reduced spin parameter. After, we look for effects on the history of each system, so we shall analyse all the parameters of the MAH (Mass Assembly History) of each pair, that is, the last major merger, the formation and the assembly time. Finally, we quantify different possible alignments of pairs regarding characteristic directions of the environment, like the eigenvectors of the chosen web scheme and the principal directions of inertia of the nearest void region.

Based on the results of Section 5, our strategy consists in using the fractional anisotropy and the distance to the nearest void region to detect any possible environmental bias on each one of the analysed properties. Furthermore, as the

two web scheme have proven to be equivalent respect the fractional anisotropy index and the statistics of void regions, we shall consider in this section only the T-web scheme. Analogously for the halo schemes, we only consider here the BDM halos.

6.1   Bias induced on kinematic and dynamics properties

Our Local Group of galaxies is certainly the most and best known large-scale structure of the universe, including the knowledge of a set of kinematic properties, that due to their mechanical nature, are easily testable by dark matter simulations like Bolshoi. The first of these properties that we analyse in this section is the total mass of the pair systems. Although there are not good enough estimates of each single mass of the host halos of the Milky Way and M31 galaxies, there is a dynamical estimate of their overall mass **[Reference here]** compatible with the selection criteria defined for selecting the `RIP` samples.

In Figure 11 we calculate the distribution of `IP` and `RIP` samples with regards to the total mass of each pair and the fractional anisotropy index of the host cell. In order to make clearer any possible correlation between these properties, in the right panel we compute individual histograms for systems selected according to defined mass ranges.

... Radial vs. tangential velocities
... Angular Momentum
... Total Mechanical energy.
... Reduced Spin

6.2   Bias induced on the Mass Assembly Histories

... Last major merger. Formation Time. Assembly Time.

6.3   Pair Alignment with the Cosmic Web

... Separation.
... Relative velocity.
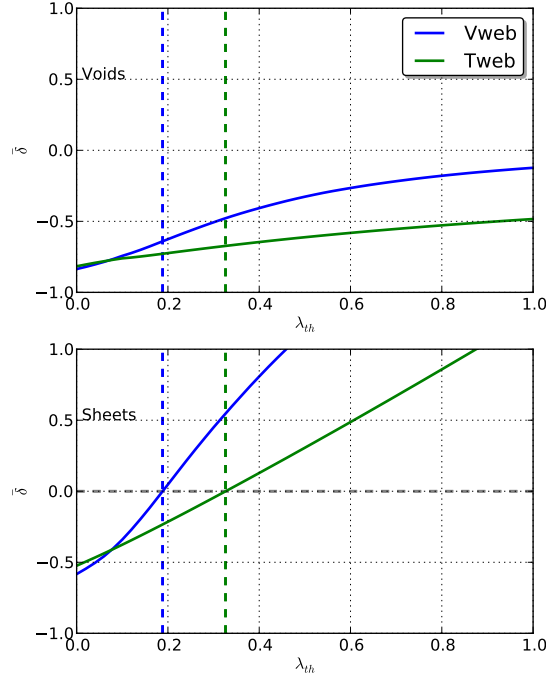... Angular Momentum.

7   CONCLUSIONS

Figure 1. Mean density parameter for each one of the defined environments according to the chosen λ_{th} value and for both classification schemes. Tweb (green lines) and Vweb (blue lines). The mean density parameter is calculated by averaging all the values of the cells determined as a certain type of environment according to its eigenvalues. The optimal parameters found are $\lambda_{opt}^{T} = 0.326$ and $\lambda_{opt}^{V} = 0.188$.
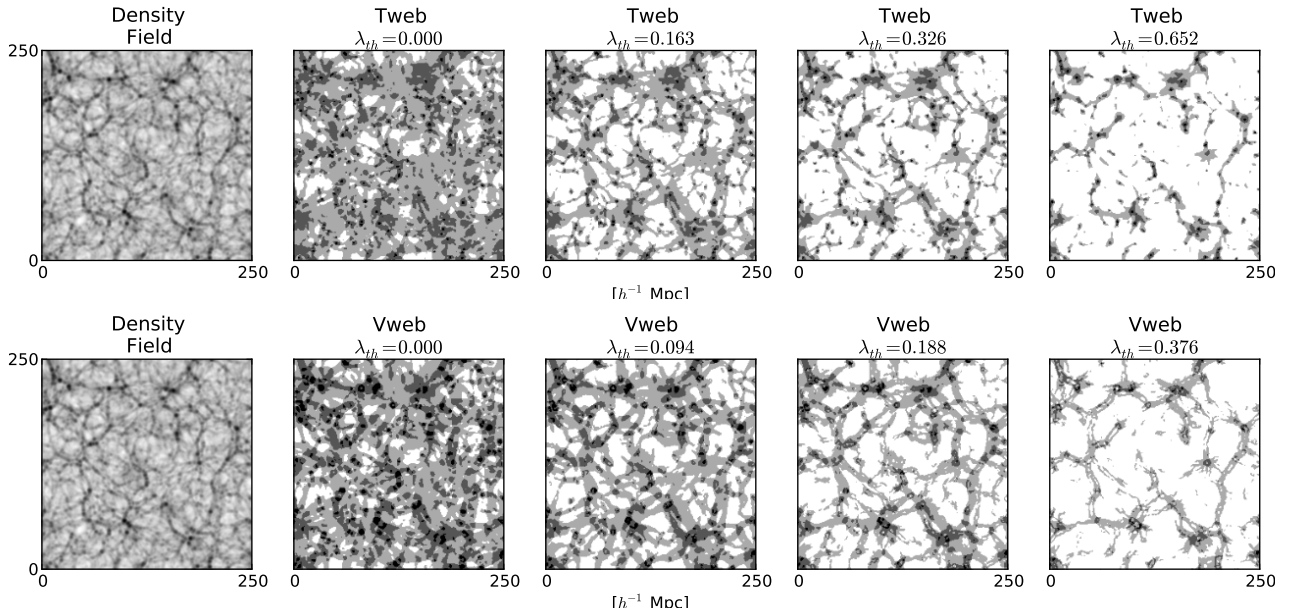

Figure 2. Visual impression of the density field (left panels), and of each classification scheme with the λ_{th} values obtained by our criteria (others panels). Our color convention for each environment is (white) - void, (light gray) - sheet, (gray) - filament, (black) - knot. For each web scheme, it has been used the previously established optimal threshold as a reference value, so plots are done with the next values $\lambda_{th} = 0.0$, $\lambda_{th} = \lambda_{opt}/2$, $\lambda_{th} = \lambda_{opt}$ and $\lambda_{th} = 2\lambda_{opt}$.
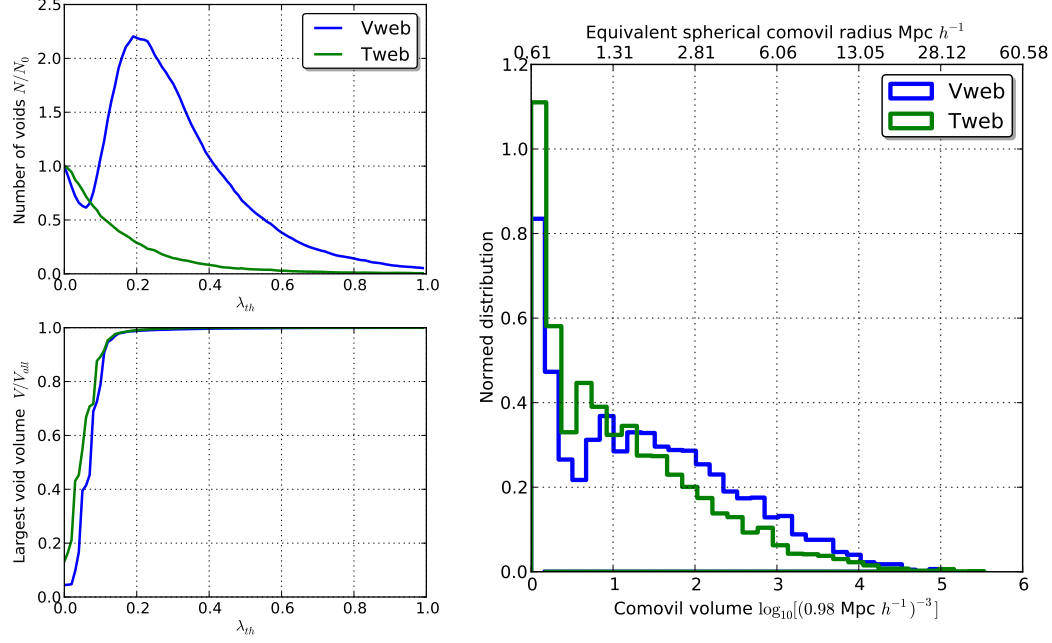
Figure 3. Percolation analysis of void regions for different λ_{th} values and for both defined classification schemes. T-web (blue lines) and V-web (green lines). Plot of the largest volume and the number of voids detected according to the threshold value λ_{th} (left panels). Size distribution histogram of void cells using the threshold value $\lambda_{th} = 0.0$ for both schemes (right panel).
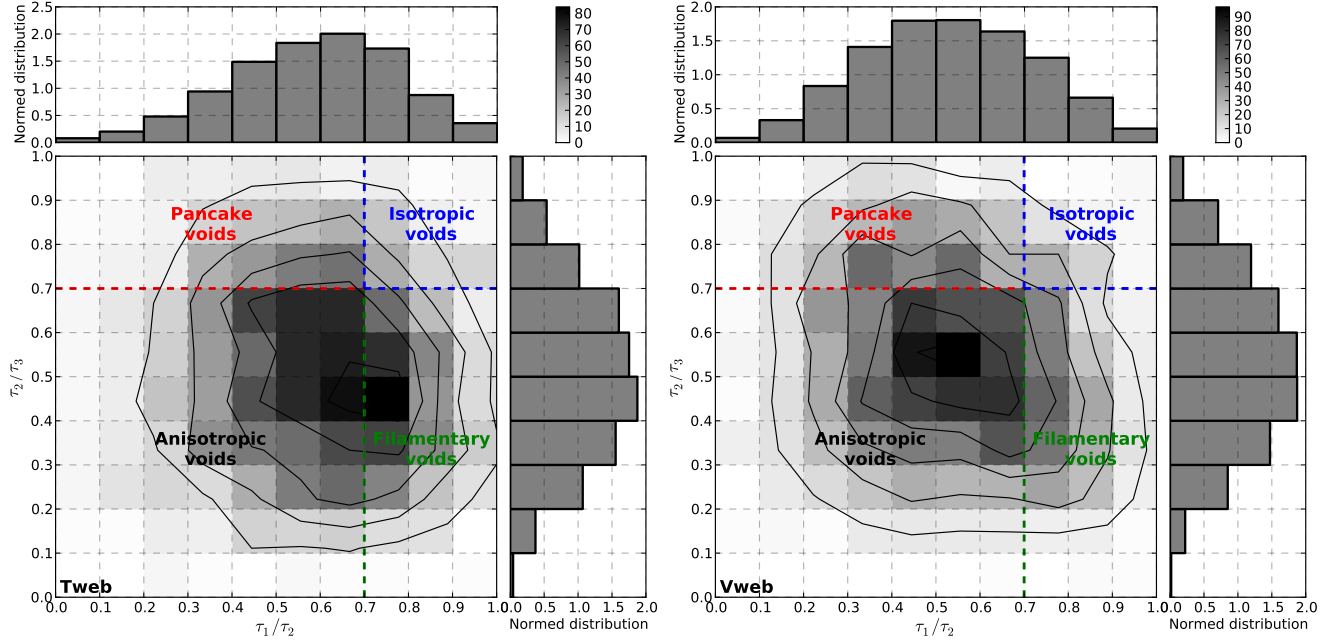

Figure 4. Histogram of eigenvalue ratio τ_1/τ_2 vs τ_2/τ_3 for the inertia tensor of void regions. T-web (left panel) and V-web (right panel). Number of cells per region in 2D histograms are indicated by the respective colour bar. Upper (τ_1/τ_2) and right (τ_2/τ_3) panels of each figure shows a normalized histogram of each ratio parameter. The adopted division for quantify the morphology of void regions is not a well justified, it must be understood as a fuzzy and continuous limit, done just for illustrative purposes.
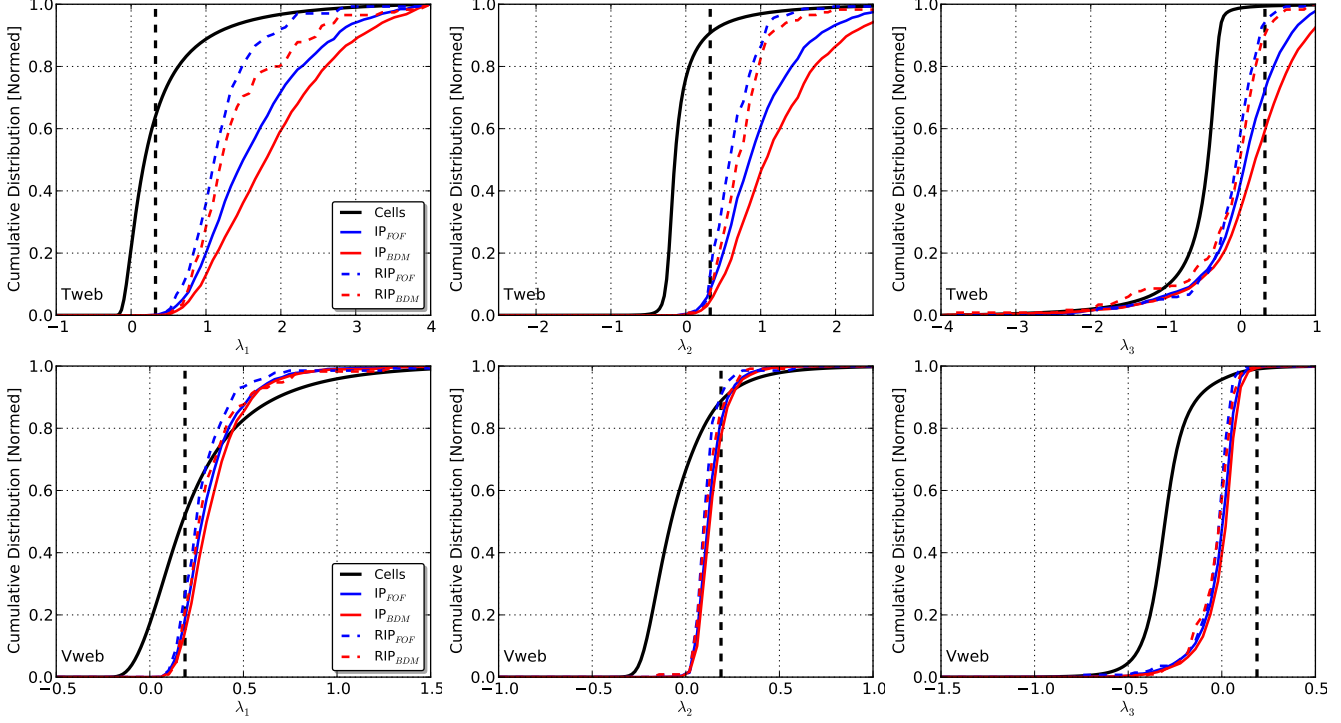
Figure 5. Distributions of eigenvalues for each defined scheme. T-web (upper panels) and V-web (lower panels). In each figure is calculated the distributions of eigenvalues for the volume cells of the simulation (black lines), evaluating the respective tensor on the geometric center of the cell. This is also done for `IP` (continuous lines) and `RIP` (dashed lines) samples (both BDM (red) and FOF (blue)), but the tensors are evaluated on the cell which contains the center of mass of the halo pair. The vertical dashed line corresponds to the optimal threshold value λ_{opt} for each scheme respectively.
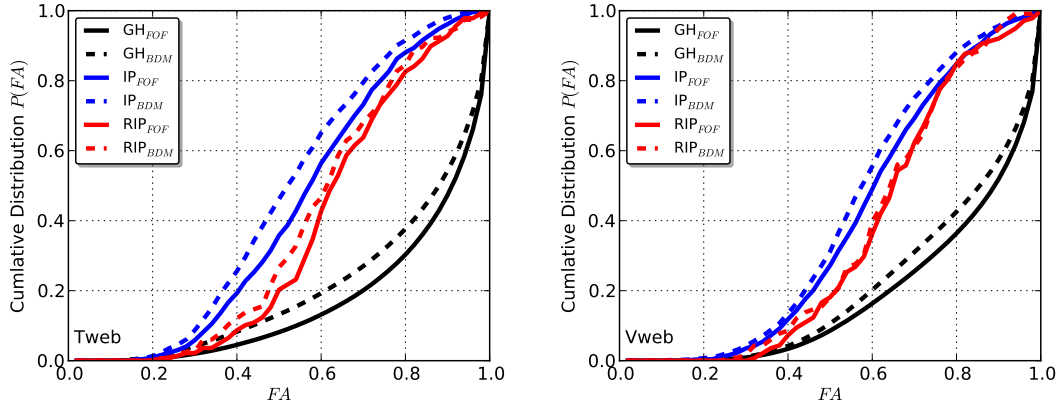
Figure 6. Cumulative distribution of the fractional anisotropy for each web scheme. T-web (right panel) and V-web (left panel). Distributions for each sample are also calculated, `GH` sample (black lines), `IP` sample (blue lines) and `RIP` sample (red lines). In order to compare each halo scheme, we also calculate distributions for each one, FOF (dashed lines) and BDM (continuous lines).
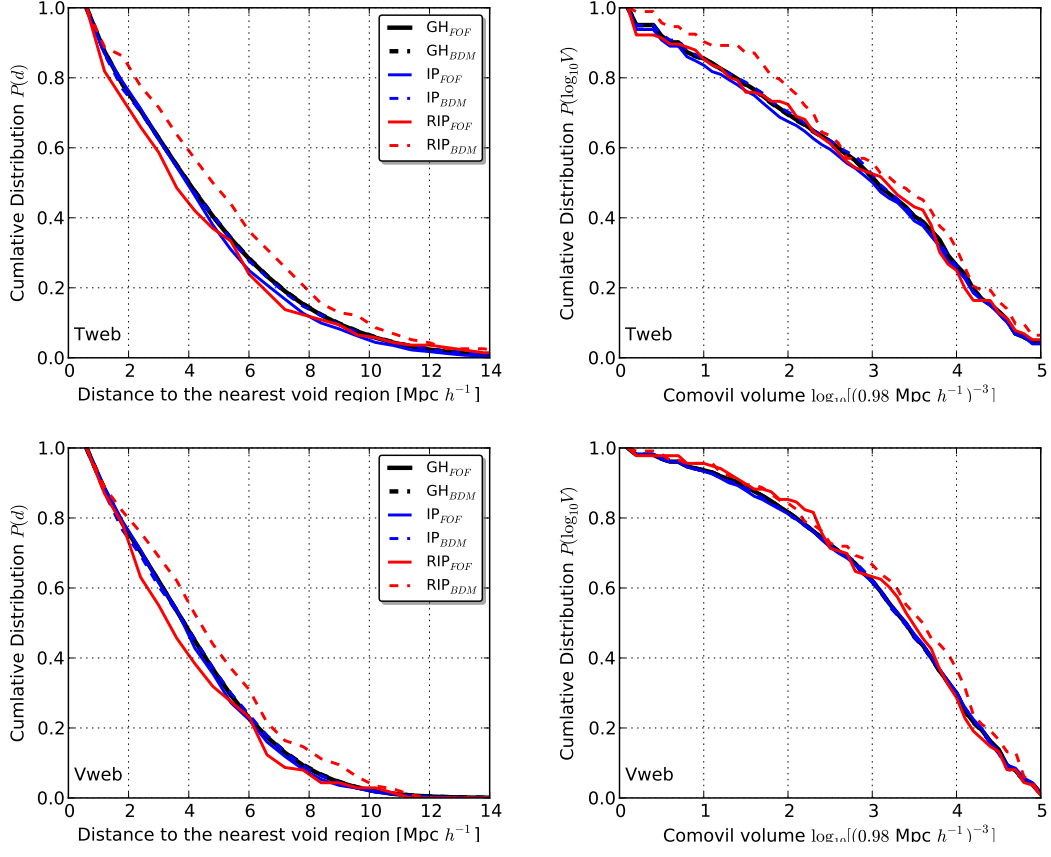
Figure 7. Cumulative distribution of distances (right panels) and volume sizes (left panels) of the nearest void region of each system and for each web scheme. T-web (upper panels) and V-web (lower panels). Systems of the `GH` sample (black lines), `IP` sample (blue lines) and `RIP` sample (red lines) are considered. It is also included both halo schemes, FOF (dashed lines) and BDM (continuous lines).
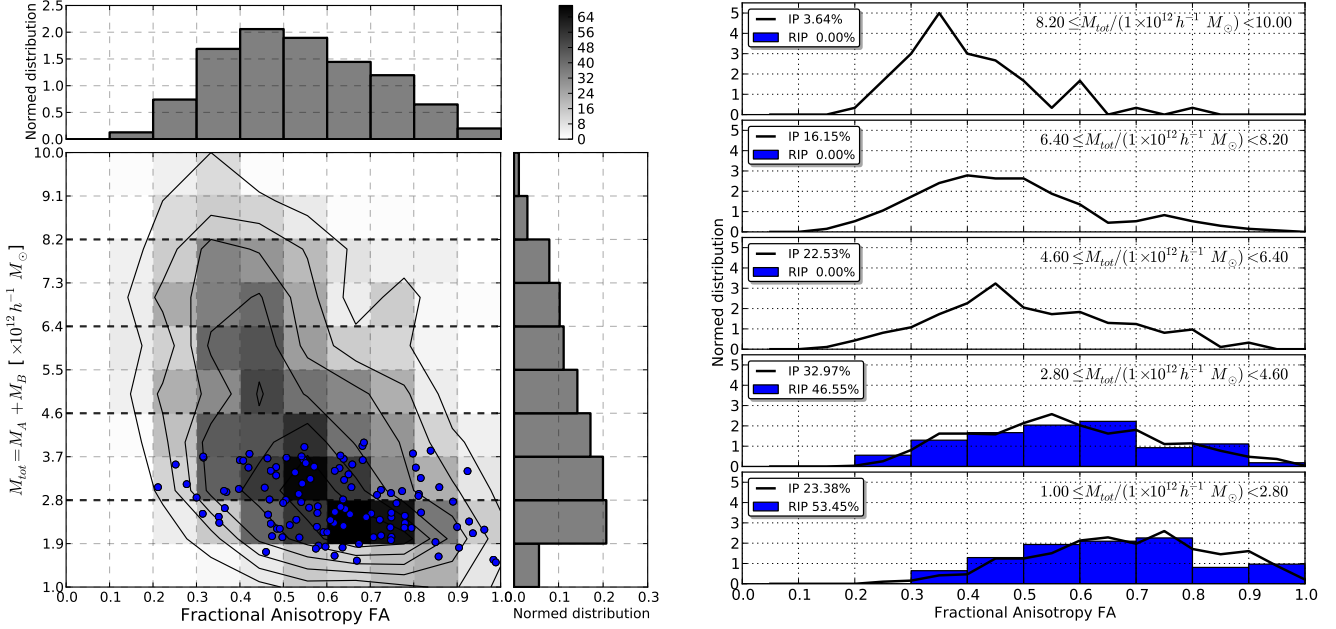
Figure 8. *Left panel:* histograms of the total mass of each pair sample, IP (2D histogram) and RIP (blue scatter), vs the fractional anisotropy index associated to each system. In the side panels we compute individual histograms of each one of the analysed properties for IP systems. *Right panel:* selecting different mass ranges for the total mass of the pairs, specified in each single panel, we calculate histograms of the fractional anisotropy of each sample, IP (black lines) and RIP (blue bars).
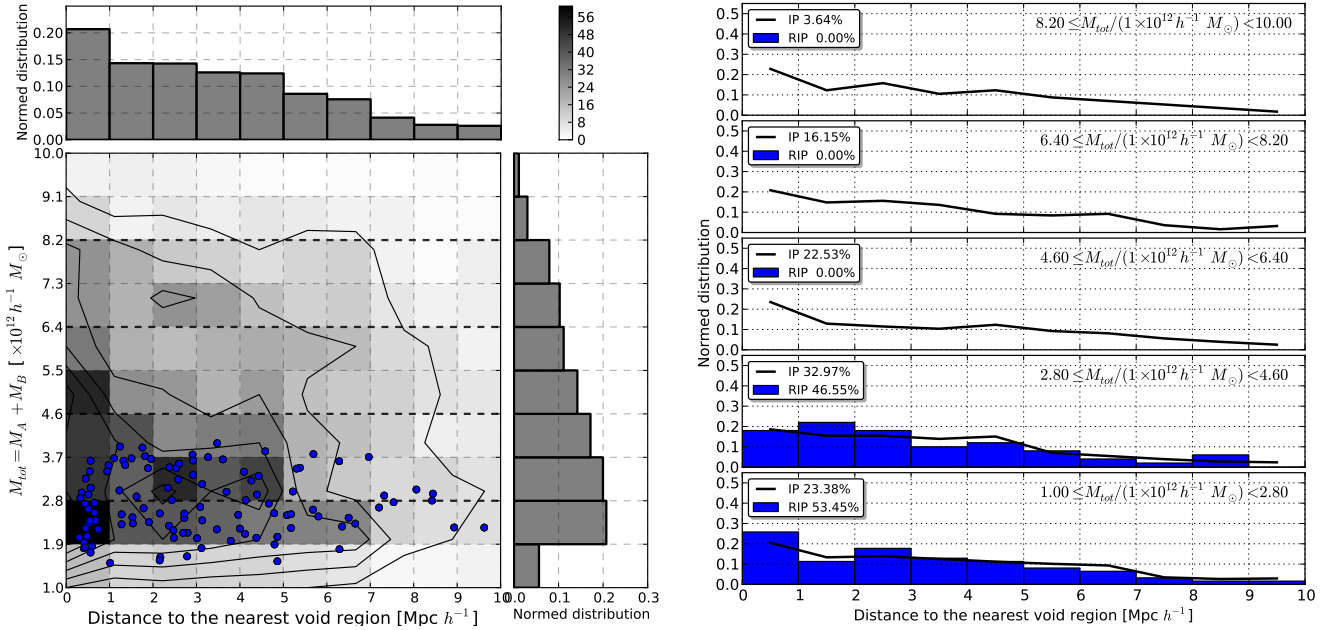

Figure 9. *Left panel:* histograms of the total mass of each pair sample, IP (2D histogram) and RIP (blue scatter), vs the distance to the nearest void region associated to each system. In the side panels we compute individual histograms of each one of the analysed properties for IP systems. *Right panel:* selecting different ranges for the mass ratio of the pairs, specified in each single panel, we calculate histograms of the distance of each sample, IP (black lines) and RIP (blue bars).
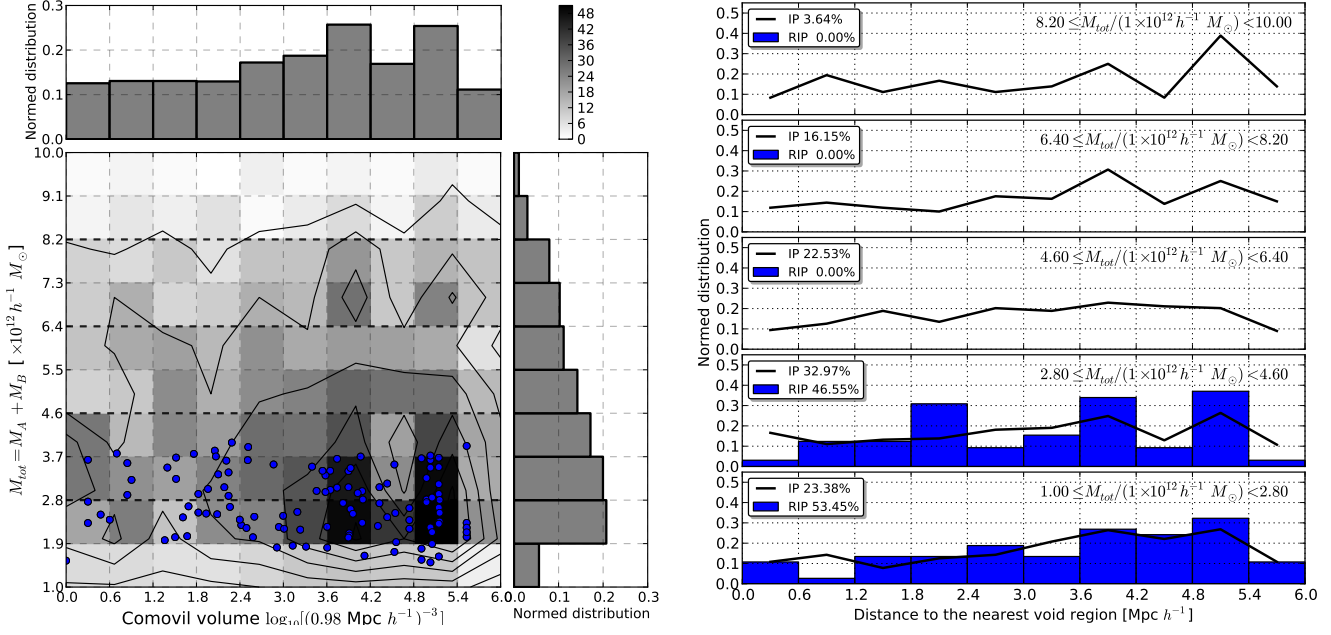
Figure 10. *Left panel:* histograms of the total mass of each pair sample, `IP` (2D histogram) and `RIP` (blue scatter), vs the distance to the nearest void region associated to each system. In the side panels we compute individual histograms of each one of the analysed properties for `IP` systems. *Right panel:* selecting different ranges for the mass ratio of the pairs, specified in each single panel, we calculate histograms of the distance of each sample, `IP` (black lines) and `RIP` (blue bars).
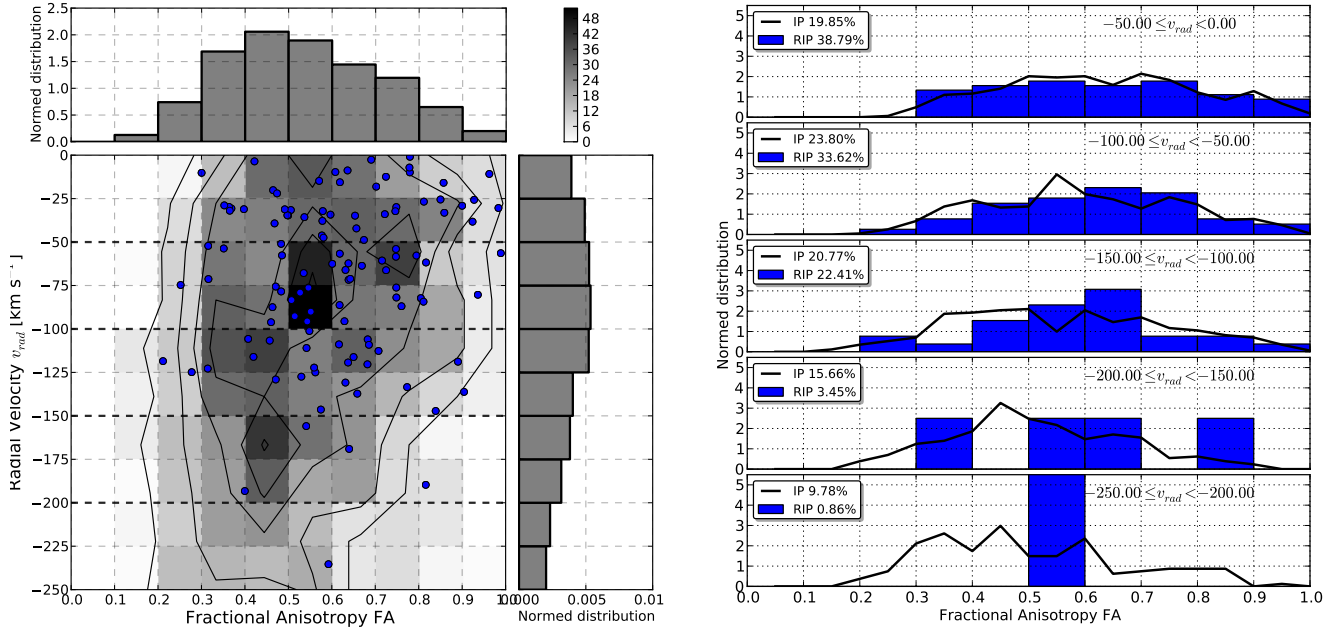

Figure 11. *Left panel:* histograms of the radial velocity of each pair sample, `IP` (2D histogram) and `RIP` (blue scatter), vs the fractional anisotropy index associated to each system. In the side panels we compute individual histograms of each one of the analysed properties for `IP` systems. *Right panel:* selecting different velocity ranges for the radial velocity of the pairs, specified in each single panel, we calculate histograms of the fractional anisotropy of each sample, `IP` (black lines) and `RIP` (blue bars).